Multi-scale drought and ocean–atmosphere variability in monsoon Asia

2015 Environ. Res. Lett. 10 074010

(http://iopscience.iop.org/1748-9326/10/7/074010)

Environmental Research Letters

LETTER

Multi-scale drought and ocean–atmosphere variability in monsoon Asia

Manuel Hernandez[1], **Caroline C Ummenhofer**[2] **and Kevin J Anchukaitis**[3]

[1] Department of Geography, Texas A&M University, College Station, TX, USA
[2] Department of Physical Oceanography, Woods Hole Oceanographic Institution, Woods Hole, MA, USA
[3] Department of Geology and Geophysics, Woods Hole Oceanographic Institution, Woods Hole, MA, USA

E-mail: mahernandez@tamu.edu

Keywords: South Asian monsoon, Monsoon Asia Drought Atlas, Strange Parallels drought, El Niño

OPEN ACCESS

RECEIVED
8 May 2015

REVISED
23 June 2015

ACCEPTED FOR PUBLICATION
2 July 2015

PUBLISHED
17 July 2015

Abstract

Spatially extensive and persistent drought episodes have repeatedly influenced human history, including the 'Strange Parallels' drought event in monsoon Asia during the mid-18th century. Here we explore the dynamics of sustained monsoon failure using observed and tree-ring reconstructed drought patterns and a 1300-year pre-industrial community earth system model control run. Both modern observational and climate model drought patterns during years with extremely weakened South Asian monsoon resemble those reconstructed for the Strange Parallels drought. Model analysis reveals that this pattern arises during boreal spring over Southeast Asia, with decreased precipitation and moisture flux, while related summertime climate anomalies are confined to the Indian subcontinent. Years with simulated South Asian drying exhibit canonical El Niño conditions over the Pacific and associated shifts in the Walker circulation. In contrast, multi-year drought periods, resembling those sustained during the Strange Parallels drought, feature anomalous Pacific warming around the dateline, typical of El Niño Modoki events.

1. Introduction

The Asian monsoon system is a large-scale coupled ocean–atmosphere phenomenon characterized by distinct seasonal precipitation and circulation features. Variability in monsoon rainfall has a significant influence on economic and agriculture production across tropical Asia. Remote oceanic influences are known to modulate the monsoon system, including the El Niño Southern Oscillation (ENSO) and Indian Ocean dipole (IOD; Ashok *et al* 2004, Ummenhofer *et al* 2011, Ummenhofer *et al* 2013; and references therein), resulting in extensive and sometimes persistent droughts (Wang 2005, Cook *et al* 2010). Pacific sea surface temperature (SST) anomalies associated with El Niño events affect the Asian monsoon through an eastward shift in the zonal Walker circulation, and anomalous subsidence over monsoon Asia (Rasmusson and Carpenter 1983, Ummenhofer *et al* 2013). More recently, variations in the location of maximum warming in the equatorial Pacific during El Niño events have been associated with regionally distinct effects on Asian monsoon variability. Canonical (eastern Pacific) El Niño and so-called El Niño Modoki events have different spatial and temporal signals (Weng *et al* 2007, Taschetto *et al* 2010). El Niño Modoki events, characterized by a warming pattern in the central Pacific, influence tropical circulation via meridional SST gradients and an anomalous two-cell Walker Circulation in the troposphere throughout the tropical Pacific (Ashok *et al* 2007, Weng *et al* 2007, Taschetto *et al* 2010, Tao *et al* 2014).

Instrumental and paleoclimate observations reveal anomalous monsoon variability across a range of spatiotemporal scales, including both interannual- and decadal-scale drought and pluvial periods (e.g. Yihui and Chan 2005, Wang *et al* 2008, Buckley *et al* 2010, Cook *et al* 2010). Severe and persistent droughts in the past in monsoon Asia are evident in tree-ring paleoclimate reconstructions, particularly from the spatiotemporal Monsoon Asia Drought Atlas (MADA). The MADA utilizes a network of more than 300 annually-resolved tree-ring width time series covering the last 700 years (Cook *et al* 2010). 'Megadroughts' of greater

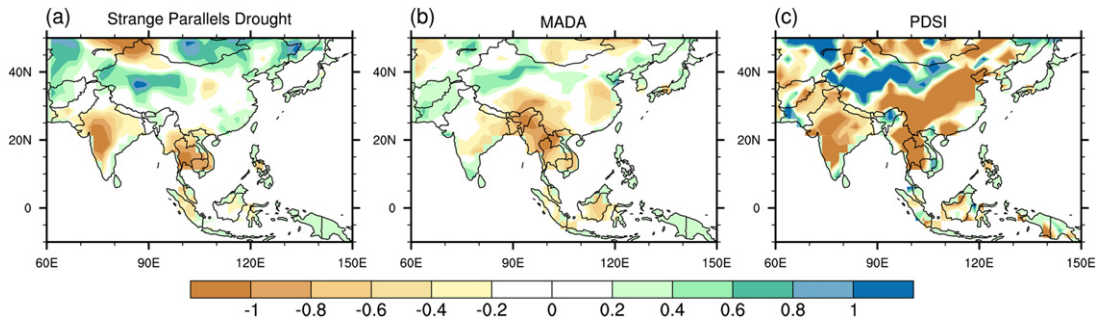

Figure 1. (a) The Strange Parallels drought (1756–1768) as seen in the MADA (Cook *et al* 2010) compared with composites of persistent weakened monsoonal years (minimum 10% of MADA) during the instrumental record (1901–2005) from (b) MADA and (c) observational PDSI (Dai 2011).

intensity and duration than those in the instrumental record are evident in these paleoclimate reconstructions, including the particularly severe, extensive, and persistent 'Strange Parallels' period (1756–1768 CE, figure 1(a)), a monsoon failure that coincided with societal upheaval and the collapse of polities in Thailand, Myanmar, and Vietnam (Cook *et al* 2010). While skillful representation of Asian monsoon variability remains a challenge for state-of-the-art general circulation models (GCMs; Turner and Annamalai 2012), paleoclimate field reconstructions, like the MADA, provide out-of-sample evaluation targets for climate models, particularly of their ability to simulate decadal-scale hydroclimate features that have societal relevance. For their part, GCMs further our understanding of the coupled ocean–atmosphere dynamics that bring about prolonged drought episodes.

We can compare the spatially broad and temporally persistent Strange Parallels drought with observed Palmer Drought Severity Index (PDSI) values (1901–2005; Dai 2011) during periods of weak monsoon circulation. Years of weakened monsoon circulation are identified using the South Asian monsoon index (SAMI), a broad-scale circulation index encompassing regions over India and Southeast Asia (70°E–110°, 10°N–30°) that measures the meridional wind shear between the lower and upper troposphere (V_{850}–V_{200}) (Goswami *et al* 1999). Composites for both paleoclimate and observations are the mean PDSI values over the boreal summer monsoon season (June–August, JJA). A MADA composite of years with weakened monsoon during the instrumental period (figure 1(b)) reveals a similar spatial drought pattern, as that reconstructed for the Strange Parallels drought (figures 1(a), and 2(b) in Cook *et al* 2010): i.e., with dry conditions in the Indian subcontinent and Southeast Asia, and wet anomalies over northern portions of the Tibetan plateau and northwest China. The instrumental PDSI also broadly reflects this drought pattern (figure 1(c)). The magnitudes seen in the MADA and instrumental PDSI differ as tree-ring reconstructions may only capture a fraction of the instrumental variance and the combination of reconstruction ensembles can further reduce the amplitude of the signal (Ummenhofer *et al* 2013).

In this paper, we assess how weakened large-scale South Asian monsoon circulation leads to both interannual and decadal-scale drought conditions, and how these are linked to the ocean–atmosphere dynamics of the Indo-Pacific system. As seen in figure 1, weak monsoon years during the instrumental period exhibit drought patterns across monsoon Asia that are reminiscent to that found during the Strange Parallels drought in the MADA. We examine the large-scale climatic conditions that could have given rise to the Strange Parallels drought, and what this reveals about the dynamics of ocean–land–atmosphere interactions as they relate to the Asian monsoon system. Given the decadal and multi-decadal nature of the Strange Parallels drought in the 18th century, the instrumental record lacks the temporal coverage necessary to explore low-frequency variations of the South Asian monsoon on such decadal to multi-decadal timescales. Instead, we use a long simulation of the National Center for Atmospheric Research (NCAR) Community Earth System Model (CESM) to identify and analyze monsoon drought patterns at both interannual and decadal time scales.

2. Datasets and methodology

The MADA (Cook *et al* 2010) is a tree-ring reconstruction of the boreal summer (JJA) PDSI, a common index of meteorological drought incorporating both precipitation and evapotranspiration used to quantify long-term changes in aridity over global land areas (Dai 2011). The MADA covers the land area across the domain 60°–145°E and 10°S–58°N at a spatial resolution of 2.5° latitude/longitude and spans from 1300 to 2005 CE. In addition to the tree-ring reconstructed PDSI, we also investigate the observed PDSI during the instrumental record (Dai *et al* 2004).

A series of monthly gridded observational and reanalysis products are used to assess the large-scale circulation of the South Asian monsoon. These include:

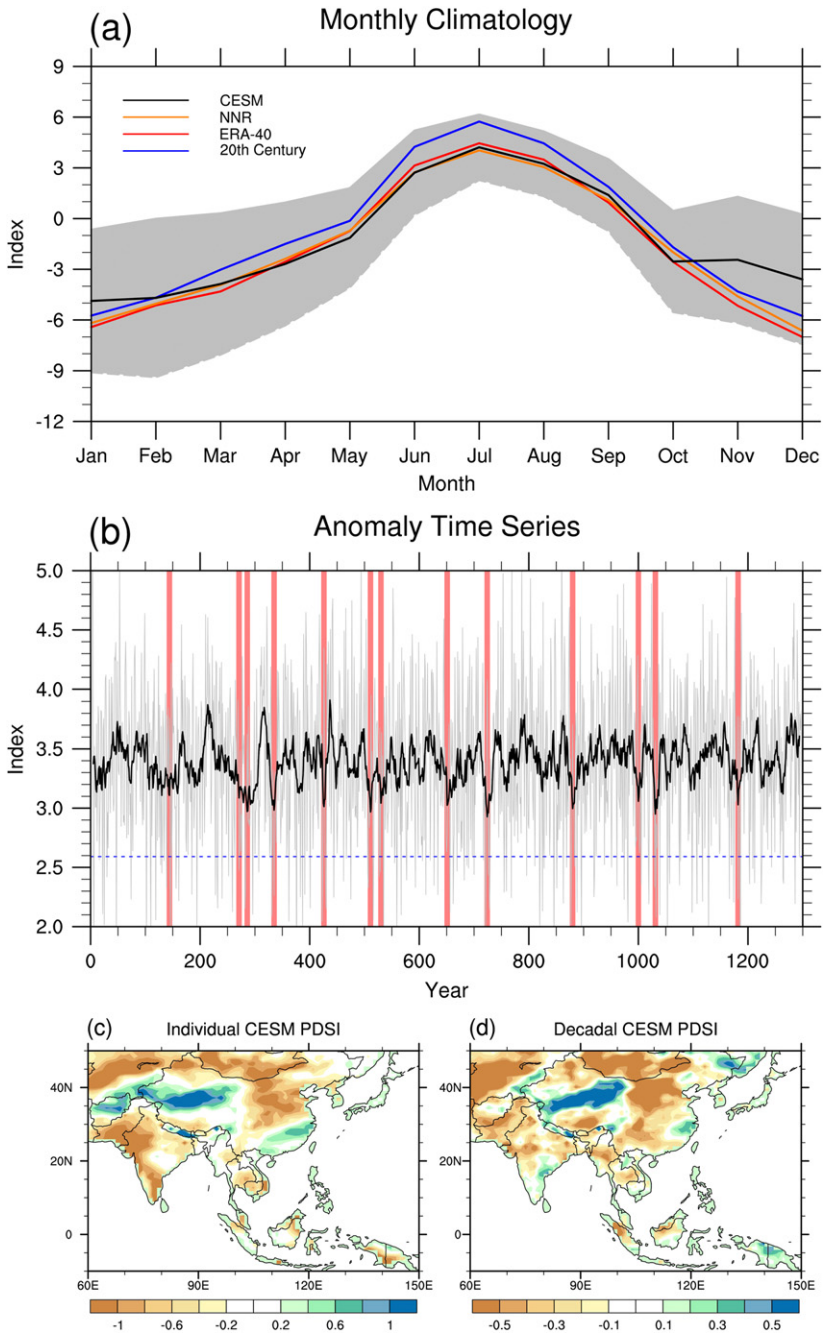

Figure 2. (a) Seasonal cycle of SAMI for NNR, ERA-40, 20th Century, and the CESM; gray shading represents ±1 standard deviation based on the CESM. (b) JJA SAMI anomaly time series, where gray indicates 'individual' years and black represents an 11-year running average. Years below the blue line are considered weakened monsoon index years ($n = 130$) for 'individual' and salmon shading for 'decadal' episodes ($n = 13$). (c), (d) CESM PDSI composite anomalies for 'individual' and 'decadal' episodes.

National Center for Environmental Prediction (NCEP)/NCAR reanalysis (NNR, Kalnay *et al* 1996, 1948–2011), the 20th Century Reanalysis (Compo *et al* 2011, 1871–2008), and the European Centre for Medium-Range Weather Forecasts ERA-40 Reanalysis (Uppala *et al* 2005, 1958–2011). We use the SAMI as a measure of monsoon circulation strength, which has previously been employed to assess monsoon strength and evaluate GCM performance (Goswami *et al* 1999).

We utilized a pre-industrial control run of 1300 years length of the NCAR CESM to understand the dynamics of South Asian monsoon variability across a range of timescales. The CESM is a state-of-the-art GCM that consists of atmosphere, land, ocean, and sea ice components (Gent *et al* 2011, Meehl *et al* 2013). The Parallel Ocean Program version 2 (POP2) has 60 vertical levels with a 1.11° zonal resolution and a meridional resolution of 0.27° at the equator, increasing to 0.54° around 33°N/S, and becoming constant at higher latitudes (Gent *et al* 2011). The Community Atmospheric Model version 4 is the atmospheric component of the CESM with a uniform spatial resolution of 1.25° × 0.9° (Gent *et al* 2011). We assess the monthly climatology from the CESM against different

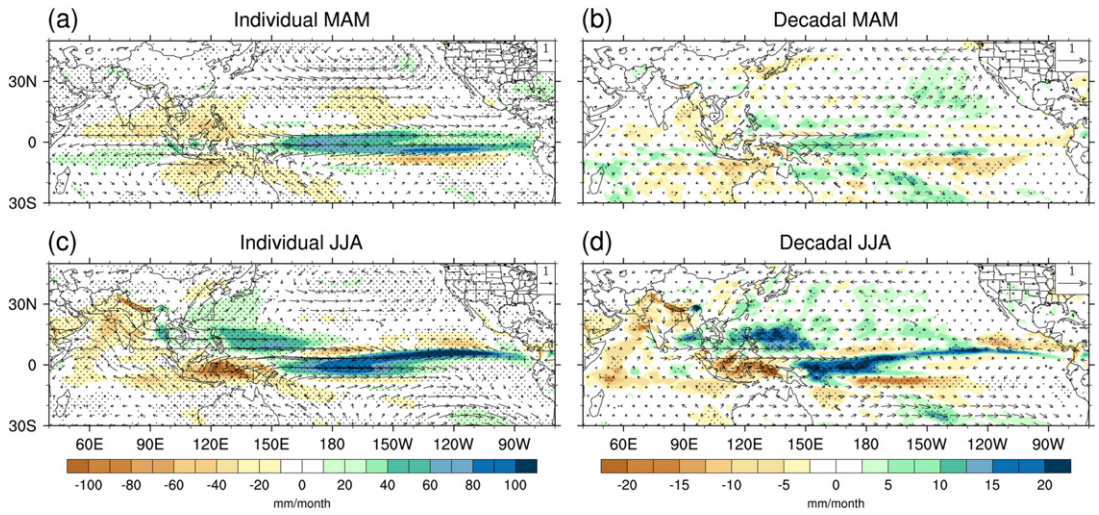

Figure 3. Composite anomalies of total precipitation (mm/month) and 850 hPa level winds (m s^{-1}) in CESM for (a), (b) MAM and (c), (d) JJA for (a), (c) individual years and (b), (d) decadal episodes of weakened monsoon circulation.

reanalysis products using the SAMI to ascertain the model's skill in representing South Asian monsoon circulation characteristics, before applying it to analysis of monsoon drought. In addition to model fields simulated in CESM, we calculate a model synthetic PDSI (Dai *et al* 2004) using simulated precipitation and temperature for direct comparison with the MADA.

We conducted a time series analysis of the simulated JJA SAMI from the pre-industrial control run of the CESM in order to identify years of persistent weakened circulation. We classified years falling below the lowest 10% SAMI threshold (blue dotted line) as years with a weakened monsoon index ($n = 130$). We also utilize an 11-year running average time series (superimposed onto the raw time series) to identify the decadal signal and capture persistent weakening in the monsoon as decadal local minima ($n = 13$; lowest 10% of average decadal SAMI values). We then calculate composites of model-derived JJA PDSI in order to assess the model's ability to simulate decadal-scale drought patterns. We evaluated the proximate and large-scale climate conditions associated with simulated monsoon drought by creating composite anomalies for these epochs of weakened monsoon circulation. We created model composite anomaly maps of total precipitation, 850 hPa-level winds, SST, and velocity potential at 200 hPa level for periods with weakened JJA monsoon circulation on both an interannual ($n = 130$) and decadal ($n = 13$) basis. In addition to examining the core JJA monsoon season, we also evaluated potential preconditioning of subsequent summer soil moisture and drought conditions during the early/pre-monsoon March–May (MAM) season. The land surface conditions prior to monsoon onset are significant in setting the land-sea thermal contrast and driving monsoon circulation.

A two-tailed t test is used to estimate the significance of climate anomalies during periods with weakened South Asian monsoon strength.

3. Results

3.1. South Asian monsoon in CESM

Overall the model simulation of the SAMI seasonal cycle aligns closely with the NNR and ERA-40 during MAM and JJA (figure 2(a)). The CESM SAMI is weaker than the 20th century reanalysis; however, the latter is anomalously strong compared to the other reanalysis products and the ±1 standard deviation of the CESM SAMI lies within the range of South Asian monsoon variability based on reanalysis products. The SAMI simulated by CESM during October–December is stronger than the three reanalysis products by 1–3 m s^{-1}, but captures well the monsoon strength during MAM and JJA, our seasons of interest here.

The pre-industrial control run of the CESM simulates periods of weakened monsoon circulation at both interannual and decadal timescale (figure 2(b)). The interannual CESM PDSI composite mimics the observed spatial drought patterns seen in the paleoclimate and instrumental observational record (figure 1), especially the signal in western India and parts of Pakistan and the excess moisture pattern over the northern regions of the Tibetan plateau (figure 2(c)). At the decadal time scale, the signal amplitude is reduced as expected, but the same coherent spatial patterns remain, including the horseshoe-shaped signal across India and Southeast Asia (figure 2(d)).

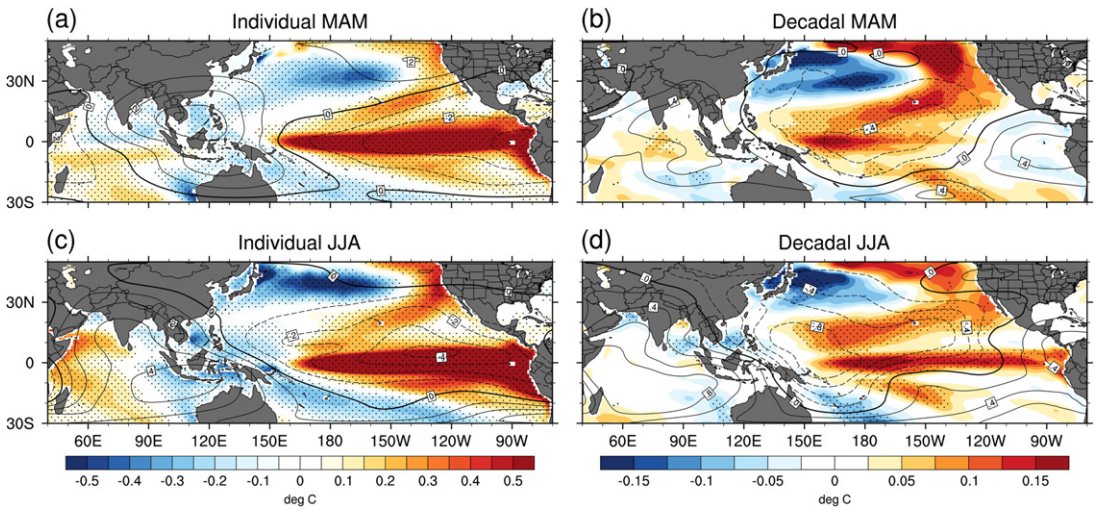

Figure 4. Composite anomalies of SSTs (°C) and velocity potential ($\times 10^6$ m^2 s^{-1}) in CESM for (a), (b) MAM and (c), (d) JJA for (a), (c) individual and (b), (d) decadal episodes with a weakened monsoon circulation.

3.2. Impact of weakened South Asian monsoon on regional climate

We examined both interannual and decadal timescales in order to identify the dynamical changes leading to the associated drought conditions over India and Southeast Asia (figure 3). For the individual years (10%, $n = 130$) with the lowest simulated SAMI index, figure 3(a) shows an associated anomalous anticyclonic rotation flow over India, with an anomalous southwest flow in northern India and northeast flow in Southeast Asia, indicative of the weakened monsoon during MAM. Modeled anomalous drying of ~40 mm/month is centered in the southern regions of Southeast Asia including Thailand, Cambodia, Vietnam, and portions of southern India, associated with weakened wind features over the Arabian Sea and South China Sea. On decadal time scales (figure 3(b)), simulated MAM wind anomalies show a similar pattern over Southeast Asia and south India, and anomalous drying of ~10 mm/month occurs over Myanmar. During JJA for simulated individual weak monsoon years (figure 3(c)), the seasonal cross-equatorial flow normally persistent during the monsoonal period weakens considerably. This closely aligns with the simulated anomalous drying pattern of ~100 mm/month constrained to India, southern Pakistan, and Nepal. In contrast, stronger winds over the Bay of Bengal result in anomalously wet (~80 mm/month) conditions over western portions of Southeast Asia. At decadal time scales (figure 3(d)), strengthened and dry northerly winds over northern India coincide with an anomalous drying signal (~20 mm/month), as well as the above-normal precipitation in Southeast Asia (~15 mm/month).

SST anomalies and velocity potential at 200 hPa are shown in figures 4(a)–(d). Interannual MAM velocity potential mirrors the anomalous precipitation distributions and SST anomalies; a warm eastern equatorial Pacific drives enhanced upward motion locally, while anomalous subsidence over Southeast Asia favors drought conditions in that region. The MAM SST anomalies are similar to an El Niño signal with an anomalous warm equatorial Pacific (~0.5 °C) and cooling patterns over the Indo-China peninsula. Furthermore, a positive IOD pattern is observed, characterized by warm (cold) SST features in the western (eastern) Indian Ocean, which can be linked to ENSO events through an extension of the Walker Circulation to the west.

Previous studies have shown the CESM to have a reasonable representation of canonical (cold-tongue) and warm-pool (Modoki) ENSO events with regard to the seasonal evolution, magnitude, and patterns compared to observations in a multi-model intercomparison of CMIP5 models (Kug *et al* 2012, Taschetto *et al* 2014). A realistic representation of the seasonal evolution of SST anomalies associated with ENSO is crucial for skillfully representing teleconnection patterns across the broader Indo-Pacific region, including monsoon Asia. Furthermore, the CESM also skillfully represents teleconnection patterns to the Austral–Asian monsoon (Jourdain *et al* 2013).

The decadal signal differs from the interannual, particularly with respect to SSTs. Regions of maximum warming are observed over the central equatorial Pacific with cooler temperatures off the equator in the eastern Pacific, similar to patterns found during El Niño Modoki events where maximum warming is centered over the dateline (e.g., Ashok *et al* 2007, Weng *et al* 2007, 2009, Ratnam *et al* 2010, Taschetto *et al* 2014). Decade-scale weak SAMI epochs are characterized by anomalous ascent, depicted by the velocity potential, as seen over the region of maximum SST warming and anomalous drying patterns driven by subsidence over Southeast Asia (figure 4(d)). During individual weak SAMI years (figure 4(c)), a similar El

Niño signal is observed with maximum warming constrained to the eastern Pacific (Weng *et al* 2007), but with a stronger downward motion over India and Indonesia.

Canonical El Niño events are associated with drought over Southeast Asia, Indonesia, northeastern China and locally over India (Ummenhofer *et al* 2013), which is also seen here in the model composites for individual years with weakened monsoon circulation. During a canonical El Niño event (figures 4(a) and (c)), a shift in the Walker Circulation, along with subsidence over Southeast Asia and anomalous upward motion over the eastern equatorial Pacific, favor a weakened monsoonal flow and reduction in moisture fluxes resulting in drought conditions (Ratnam *et al* 2010, Ummenhofer *et al* 2013). Interestingly, during individual weak SAMI years (figure 3(a)), below-normal precipitation is spread throughout south India and Southeast Asia, while below-normal JJA precipitation is confined to India only. This appears to also be consistent with the sensitivity of Southeast Asian tree-ring chronologies to early monsoon season moisture (Buckley *et al* 2010). Previous studies have shown a seasonal phase-locking signal for El Niño including an intensification in late summer to early fall, peak in winter, and decay in the following spring (Weng *et al* 2007, Tao *et al* 2014). In contrast, El Niño Modoki events show a different temporal signal, along with remote ocean SST distribution and global impacts. Tao *et al* (2014) described the differences between the two types of El Niño, including the change in the position of anomalous vertical motion over the Pacific Ocean, which stem from the anomalous Walker Circulation during both types of events, as well as zonal SST gradients in the eastern equatorial Pacific. Furthermore, a less coherent phase-locking signal and large decadal variability is detected for El Niño Modoki (Weng *et al* 2007). Marathe *et al* (2015) have shown El Niño Modoki events to differ from the canonical El Niños in their seasonal evolution and teleconnections, including their dynamic and thermodynamic air-sea coupling strength.

Our decadal weak monsoon composites from CESM are associated with an El Niño Modoki with maximum warming in central Pacific SSTs and rising motion over these warmer SSTs and sinking motion over the Indian region that are associated with below-normal precipitation. At annual time scales, anomalous SSTs in the Indian Ocean are much more pronounced due to internal oceanic processes including El Niño-induced Rossby wave propagations (Tao *et al* 2014). For decadal SST composites, anomalies over the Indian Ocean are less pronounced. This could be a result of a lack of significant wave propagation, like that observed during a canonical El Niño event, causing subtle SST anomalies over the Indian Ocean after an El Niño Modoki event (Tao *et al* 2014). Other studies have proposed possible mechanisms connecting decadal changes in the ENSO-monsoon system to other components of large-scale ocean–atmosphere variability, including an important role for unforced variability (Li and Ting 2015). The occurrence and persistence of El Niño Modokis in the early 20th century have demonstrated a role of multi-decadal natural climate variability can have in generating El Niño Modokis (Pascolini-Campbell *et al* 2015). Considerable multi-decadal variability in the frequency of El Niño Modoki events in the observational record has also been described, with El Niño Modoki events more common in recent decades (e.g., Ashok *et al* 2007, Yeh *et al* 2011). Such decadal modulation of ENSO characteristics (intensity, spatial distribution, and frequency of the two types) has been attributed to decadal variations in the climate mean state in the Pacific thermocline structure (e.g., Choi *et al* 2012). However, improved quantification of the effects of decadal variability in the past is needed to determine its future behavior in light of anthropogenic climate change (Turner and Annamalai 2012).

4. Conclusion

We have identified large-scale climate conditions that can lead to extensive decadal-scale monsoon drought conditions, like those that have been reconstructed using tree-rings during the mid-18th century Strange Parallels drought, an extended period of apparently weak monsoons that may have played an important role in shaping historic regional sociopolitical change (Lieberman 2003, Cook *et al* 2010). The use of the long pre-industrial control run of the CESM, combined with analysis of paleoclimate drought reconstructions, allows us to develop dynamically-based inferences about causal mechanisms across multiple time scales. Simulated patterns of PDSI from CESM are analogous to those reconstructed for the Strange Parallels epoch and the model critically provides the physical basis for interpreting these rare past events in the context of the large-scale ocean–atmosphere circulation.

Our study reveals the influence of two different types of El Niño (canonical El Niño and El Niño Modoki) on drought conditions over monsoon Asia. Canonical eastern Pacific El Niño events can have a substantial influence on interannual variability in monsoon rains; however, decadal-scale drought, like those reconstructed during the mid-18th century, appear to be associated with SST and circulation anomalies similar to El Niño Modoki, which exhibits a larger decadal signal (Weng *et al* 2007). The different Walker circulation anomalies of the two El Niños result in the distinct patterns in space and time of below-normal precipitation and drought conditions across India and Southeast Asia. Thus, our study provides the foundation for explaining mechanisms that can lead to sustained decadal drought patterns throughout monsoon Asia and confirms the

importance of the ENSO characteristics in determining spatiotemporal anomalies of the Asian monsoon system.

Acknowledgments

This work was performed with support and funding from the Significant Opportunities in Atmospheric Research and Sciences Program (NSF AGS-1120459), WHOI Academic Programs Office Funds, and NSF AGS-1338734, AGS-1203704, and AGS-1304245. This study obtained the MADA from www.ncdc.noaa.gov/paleo/pubs/cook2010/cook2010.html, the ECMWF ERA-40 Reanalysis from http://apps.ecmwf.int/datasets/data/era40_moda/?levtype=pl, the 20th Century Reanalysis from www.esrl.noaa.gov/psd/data/20thC_Rean/, the NNR from www.esrl.noaa.gov/psd/data/reanalysis/reanalysis.shtml, the PDSI from www.cgd.ucar.edu/cas/catalog/climind/pdsi.html, and the CESM from www.cesm.ucar.edu/experiments/cesm1.0/. Comments by two anonymous reviewers that helped improve an earlier version of the manuscript are gratefully acknowledged.

References

Ashok K, Behera S K, Rao S A, Weng H and Yamagata T 2007 El Niño Modoki and its possible teleconnection *J. Geophys. Res.* **112** C11007

Ashok K, Guan Z, Saji N H and Yamagata T 2004 Individual and combined influences of the ENSO and Indian ocean dipole on the Indian summer monsoon *J. Clim.* **17** 3141–55

Buckley B M, Anchukaitis K J, Penny D, Fletcher R, Cook E R, Sano M, Wichienkeeo A, Minh T T and Hong T M 2010 Climate as a contributing factor in the demise of Angkor, Cambodia *Proc. Natl Acad. Sci. USA* **107** 6748–52

Choi J, An S–I and Yeh S–W 2012 Decadal amplitude modulation of two types of ENSO and its relationship with the mean state *Clim. Dyn.* **38** 2631–44

Compo G P *et al* 2011 The twentieth century reanalysis project *Q. J. R. Meteorol. Soc.* **137** 1–28

Cook E R, Anchukaitis K J, Buckley B M, D'Arrigo R D D, Jacoby G C and Wright W E 2010 Asian monsoon failure and megadrought during the last millennium *Science* **328** 486–9

Dai A 2011 Drought under global warming: a review *WIREs Clim. Change* **2** 45–65

Dai A, Trenberth K E and Qian T 2004 A global dataset of palmer drought severity index for 1870–2002: relationship with soil moisture and effects of surface warming *J. Hydrometeorol.* **5** 1117–29

Gent P *et al* 2011 The community climate system model version 4 *J. Clim.* **24** 4973–91

Goswami B N, Krishnamurthy V and Annamalai H 1999 A broad-scale circulation index for the interannual variability of the Indian Summer Monsoon *Q. J. R. Meteorol. Soc.* **125** 611–33

Jourdain N C, Sen Gupta A, Taschetto A S, Ummenhofer C C, Moise A F and Ashok K 2013 The Indo–Australian monsoon and its relationship to ENSO and IOD in reanalyses and the CMIP3/CMIP5 simulations *Clim. Dyn.* **41** 3073–102

Kalnay E *et al* 1996 The NCEP/NCAR 40-year reanalysis project *Bull. Am. Meteorol. Soc.* **77** 437–71

Kug J–S, Ham Y–G, Lee J–Y and Jin F–F 2012 Improved simulation of two types of El Niño in CMIP5 models *Environ. Res. Lett.* **7** 034002

Li X and Ting M 2015 Recent and future changes in the Asian monsoon—ENSO relationship: natural or forced? *Geophys. Res. Lett.* **42** 3502–12

Lieberman V 2003 Strange parallels *Integration of the Mainland: Southeast Asia in Global Context* vol 1 (Cambridge: Cambridge University Press) pp 800–1830

Marathe S, Karumuri A, Swapna P and Sabin T P 2015 Revisiting El Niño Modokis *Clim. Dyn.* at press (doi:10.1007/s00382-015-2555-8)

Meehl G A, Washington W M, Arblaster J M, Hu A, Tang H, Kay J E, Gettelman A, Lawrence D M, Sanderson B M and Straind W G 2013 Climate change projections in CESM1 (CAM5) compared to CCSM4 *J. Clim.* **26** 6287–308

Pascolini-Campbell M, Zanchettin D, Bothe O, Timmreck C, Matei D, Jungclaus J H and Graf H–F 2015 Toward a record of central Pacific El Niño events since 1880 *Theor. Appl. Climatol.* **119** 379–89

Rasmussen E M and Carpenter T H 1983 The relationship between eastern equatorial Pacific sea surface temperature and rainfall over India and Sri Lanka *Mon. Weather Rev.* **110** 354–84

Ratnam J V, Behera S K, Masumoto Y, Takahashi K and Yamagata T 2010 Pacific ocean origin for the 2009 Indian summer monsoon failure *Geophys. Res. Lett.* **37** 1–6

Tao W, Huang G, Hu K, Qu X, Wen G and Gong Y 2014 Different influences of two types of El Niños on the Indian ocean SST variations *Theor. Appl. Climatol.* **117** 475–84

Taschetto A S, Sen Gupta A, Jourdain N, Santoso A, Ummenhofer C C and England M H 2014 Cold tongue and warm pool ENSO events in CMIP5: mean state and future projections *J. Clim.* **27** 2861–85

Taschetto A S, Haarsma R J, Gupta A S, Ummenhofer C C, Hill K J and England M H 2010 Australian monsoon variability driven by a Gill–Matsuno type response to central-west Pacific warming *J. Clim.* **23** 4717–36

Turner A G and Annamalai H 2012 Climate change and the South Asian summer monsoon *Nat. Clim. Change* **2** 587–95

Ummenhofer C C, D'Arrigo R D, Anchukaitis K J, Buckley B M and Cook E R 2013 Links between Indo–Pacific climate variability and drought in the monsoon Asia drought *Atlas Clim. Dyn.* **40** 1319–34

Ummenhofer C C, Sen Gupta A, Li Y, Taschetto A S and England M H 2011 Multi-decadal modulation of the El Niño-Indian monsoon relationship by Indian ocean variability *Environ. Res. Lett.* **6** 1–8

Uppala S M *et al* 2005 The ERA-40 re-analysis *Q. J. R. Meteorol. Soc.* **131** 2961–3012

Wang B 2005 *The Asian Monsoon* 1st edn (Berlin: Springer) pp 864

Wang B, Zhiwei W, Li J, Liu J, Chang C, Ding Y and Wu G 2008 How to measure the strength of the East Asian summer monsoon *J. Clim.* **21** 4449–63

Weng H, Ashok K, Behera S K, Rao S A and Yamagata T 2007 Impacts of recent El Niño Modoki on dry/wet conditions in the Pacific rim during boreal summer *Clim. Dyn.* **29** 113–29

Yeh S–W, Kirtman B P, Kug J–S, Park W and Latif M 2011 Natural variability of the central Pacific El Niño event on multicentennial timescales *Geophys. Res. Lett.* **38** L02704

Yihui D and Chan J C L 2005 The East Asian summer monsoon: an overview *Meteorol. Atmos. Phys.* **89** 117–42